PAPER

# Investigation of superconducting gap structure in HfIrSi using muon spin relaxation/rotation

IOP Publishing Journal of Physics: Condensed Matter
J. Phys.: Condens. Matter **32** (2020) 085601 (8pp) https://doi.org/10.1088/1361-648X/ab549e

# Investigation of superconducting gap structure in HfIrSi using muon spin relaxation/rotation

**A Bhattacharyya[1], K Panda[1], D T Adroja[2,3], N Kase[4], P K Biswas[2], Surabhi Saha[5], Tanmoy Das[5], M R Lees[6] and A D Hillier[2]**

[1] Department of Physics, Ramakrishna Mission Vivekananda Educational and Research Institute, Howrah 711202, West Bengal, India
[2] ISIS Facility, Rutherford Appleton Laboratory, Chilton, Didcot Oxon, OX11 0QX, United Kingdom
[3] Highly Correlated Matter Research Group, Physics Department, University of Johannesburg, PO Box 524, Auckland Park 2006, South Africa
[4] Department of Applied Physics, Tokyo University of Science, Tokyo, 125-8585, Japan
[5] Department of Physics, Indian Institute of Science, Bangalore 560012, India
[6] Department of Physics, University of Warwick, Coventry CV4 7AL, United Kingdom

E-mail: amitava.bhattacharyya@rkmvu.ac.in and tnmydas@gmail.com

Received 9 July 2019, revised 27 September 2019
Accepted for publication 5 November 2019
Published 20 November 2019

**Abstract**

We have investigated the superconducting state of HfIrSi using magnetization, specific heat, muon spin rotation and relaxation ($\mu$SR) measurements. Superconductivity was observed at $T_C = 3.6(1)$ K in both specific heat and magnetization measurements. From an analysis of the transverse-field $\mu$SR data, it is clear that the temperature variation of superfluid density is well fitted by an isotropic Bardeen–Cooper–Schrieffer (BCS) type *s*-wave gap structure. The superconducting carrier density $n_s = 6.6(1) \times 10^{26}$ m$^{-3}$, the magnetic penetration depth, $\lambda_L(0) = 259(4)$ nm, and the effective mass, $m^* = 1.57(3)\ m_e$, were calculated from the TF-$\mu$SR data. Zero-field $\mu$SR data for HfIrSi reveal the absence of any spontaneous magnetic moments below $T_C$, indicating that time-reversal symmetry (TRS) is preserved in the superconducting state of HfIrSi. Theoretical investigations suggest that the Hf and Ir atoms hybridize strongly along the *c*-axis, and that this is responsible for the strong three-dimensionality of this system which screens the Coulomb interaction. As a result, despite the presence of *d*-electrons in HfIrSi, these correlation effects are weakened, making the electron-phonon coupling more important.

Keywords: ternary equiatomic superconductor, superconducting gap structure, muon spin spectroscopy

(Some figures may appear in colour only in the online journal)

## 1. Introduction

In recent years, the ternary equiatomic phosphides, arsenides, and silicides containing elements with 4*d* or 5*d* electrons, $MM'X$, (where $M$ = transition metals such as Zr, Mo, or Hf, $M'$ = transition metals such as Ru, Rh, or Os, and $X$ = As, P, or Si) have attracted considerable attention due to their unusual superconducting properties [1–12]. These 111 materials crystallize into one of two types of layered structure: either (i) a hexagonal (*h*) $Fe_2P$-type (space group $P\bar{6}m2$) [1, 2, 10–12], or (ii) an orthorhombic (*o*) $Co_2Si$-type (space group *Pnma*) [1, 2, 8, 10, 12]. At high temperatures and pressures the orthorhombic phase modifies to the higher-symmetry hexagonal structure. The observation of superconductivity with transition temperatures ($T_C$) of more than 10 K in the 111-based phosphides [1] spurred research on similar compounds

 

formed by replacing one or more of the elements in the material. Superconductivity at temperatures as high as 12 K for *h*-ZrRuAs [3], 13 K for *h*-ZrRuP [5] and 15.5 K for *h*-MoNiP and *h*-MoRuP [10], have since been reported. Shirotani *et al* studied the superconductivity in both *h*-ZrRu*X* ($X$ = P, As or Si) and *h*-HfRuP [6, 9]. The sites within the *ab* planes of the hexagonal structure are occupied by either *M* (=Zr or Hf) and *X* atoms or Ru and *X* atoms, and two-dimensional triangular clusters of $Ru_3$ are formed. The Ru–Ru distances in these clusters are shorter than in pure Ru and it is suggested that this contraction increases the density of states (DOS) at the Fermi level, $E_F$, enhancing $T_C$ [1, 6].

Among the orthorhombic $Co_2P$-type superconductors, *o*-MoRuP has the highest $T_C$ of 15.5 K [10]. A higher value for the DOS at the Fermi level, which is dominated by the Mo-4*d* orbitals, are directly linked with the higher $T_C$ [14]. Ching *et al* [12] calculated the DOS at the Fermi level for *o*-MoRuP as 0.46 states/eV atom and predicted that *h*-MoRuP may have a $T_C$ above 20 K if the lattice dynamics and the electron-phonon coupling in *o*-ZrRuP, *o*-MoRuP, *h*-MoRuP, and *h*-ZrRuP behave in a similar way. Wong-Ng *et al* [15] also suggested that changes in $T_C$ in these superconductors are driven by changes in the DOS at the Fermi level. Recently, Kase *et al* reported superconductivity in the 111 5*d* transition metal compound *o*-HfIrSi [13]. As spin–orbit coupling (SOC) is directly proportional to $Z^4$, where $Z$ is the atomic number, spin–orbit coupling may be expected to be important in *o*-HfIrSi [16] due to the high atomic numbers of Hf and Ir. Strong SOC can have a profound effect on the properties of a superconductor. For example, Bhattacharyya *et al* [17–19] have shown that in the cage-type superconductors $R_5Rh_6Sn_{18}$ ($R$ = Lu, Sc, and Y), time-reversal symmetry (TRS) is broken due to strong spin–orbit coupling, while Yuan *et al* revealed a crossover from singlet to triplet superconductivity in noncentrosymmetric $Li_2Pd_{3-x}Pt_xB$ due to the larger SOC in $Li_2Pt_3B$ [20].

In order to shed light on the pairing mechanism in *o*-HfIrSi, and to investigate whether spin–orbit coupling influences the superconducting properties of *o*-HfIrSi, we report a comprehensive experimental study of this material using heat capacity, magnetization, and zero-field (ZF) and transverse-field (TF) muon spin relaxation/rotation ($\mu$SR) measurements. These measurements are complemented by density-functional theory (DFT) calculations of the electronic structure of HfIrSi. ZF-$\mu$SR data revealed no evidence for any spontaneous magnetic moment below $T_C$, indicating that TRS is preserved in *o*-HfIrSi. The temperature dependence of the superfluid density determined from the TF-$\mu$SR and heat capacity data indicate that HfIrSi is an *s*-wave BCS superconductor with a single isotropic energy gap. Our DFT calculations provide possible reasons for the limited effect that SOC has on the superconducting properties of HfIrSi.

## 2. Experimental details

A polycrystalline sample of orthorhombic HfIrSi was prepared by melting stoichiometric quantities of high purity Hf, Ir, and Si on a water-cooled copper hearth, under an argon atmosphere in an arc furnace. The as-cast ingot was turned and remelted several times to improve the phase homogeneity. The sample was then annealed in a evacuated quartz tube for 168 hrs at 1273 K. Powder x-ray diffraction data were collected using a RAD-2X Rigaku x-ray diffractometer. The superconducting properties of the sample were characterized via dc magnetic susceptibility measurements made using a Quantum Design, Magnetic Property Measurement System (MPMS), over the temperature range 1.5–10 K in an applied magnetic field 10 Oe. Heat capacity measurements were performed down to 0.3 K using a Quantum Design Physical Property Measurement System (PPMS) with a $^3$He insert.

Muon spin rotation and relaxation are very sensitive local probes which can be used to resolve the nature of the pairing symmetry in superconductors [21, 22]. To examine the superconducting pairing symmetry in HfIrSi, TF and ZF $\mu$SR experiments were performed using the MUSR spectrometer [22] on the muon beam line of the ISIS Pulsed Neutron and Muon Facility at the Rutherford Appleton Laboratory, United Kingdom. The high-quality polycrystalline sample of HfIrSi was mounted on a silver plate (99.995%) using low-temperature GE varnish and covered with silver foil. The sample was cooled to temperatures as low as 50 mK using a dilution refrigerator. 100% spin-polarized positive muons ($\mu^+$) were implanted into the sample and each $\mu^+$ decays with a mean lifetime of 2.2 $\mu$s releasing a positron. Given that the positrons emit along the muon spin direction, the asymmetry in positron emission direction, $P_z(t)$, is a direct measure of the muon spin polarization. The time-dependent asymmetry $A(t)$ which is proportional to $P_z(t)$ was measured using $A(t) = [N_F(t) - \alpha N_B(t)]/[N_F(t) + \alpha N_B(t)]$, where $N_B(t)$ and $N_F(t)$ are the number of positrons counted in the backward and forward detectors, respectively, and $\alpha$ is an instrumental calibration constant determined in the normal state in a small (20 G) transverse magnetic field. All the $\mu$SR data were analyzed using the WiMDA data analysis program [23]. The TF-$\mu$SR data were collected at different temperatures between 0.05 and 4 K in a transverse-field of 300 Oe ($>H_{c1}$ which is $\approx$10 Oe at 0.5 K). The ZF data were collected between 0.1 and 4 K and active compensation coils were used during these ZF measurements to reduce any stray magnetic field at the sample position to below $\sim$0.001 Oe.

## 3. Results and discussion

### 3.1. Magnetization and specific heat

HfIrSi crystallizes in an orthorhombic structure with space group *Pnma* (No. 62) [13, 16]. Powder x-ray diffraction showed the lattice parameters are $a = 6.523(5)$ Å, $b = 3.912(3)$ Å and $c = 7.353(4)$ Å. The temperature ($T$) dependence of the magnetic susceptibility, $\chi(T)$, of HfIrSi in an applied magnetic field of 10 Oe is shown in figure 1(a). $\chi(T)$ reveals a clear signature of superconductivity below a superconducting transition temperature, $T_C = 3.6(1)$ K. The magnetization, $M$, versus field, $H$, curve shown in figure 1(b) at 0.5 K is typical of type II superconductivity. The lower critical

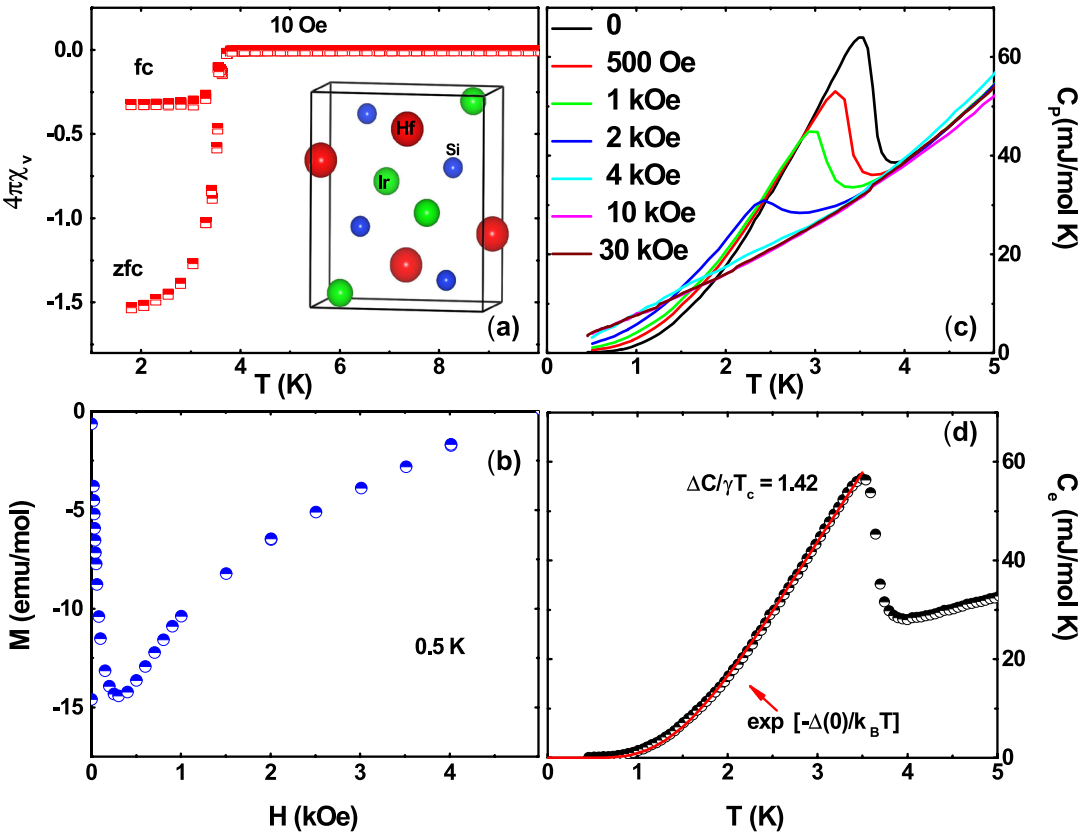


**Figure 1.** (a) Magnetic susceptibility as a function of temperature, $\chi(T)$, collected in zero-field-cooled (ZFC) and field-cooled (FC) modes in an applied field of 10 Oe in SI units. The inset shows a unit cell of the orthorhombic crystal structure (*Pnma*) of HfIrSi. (b) Isothermal field dependence of the magnetization of HfIrSi at 0.5 K. (c) Temperature dependence of heat capacity, $C_P(T)$, for $0.45 \leqslant T \leqslant 5$ K measured in different applied magnetic fields. (d) Electronic contribution to the zero-field heat capacity, $C_e$, as a function of temperature. The solid line indicates a fit to $C_e(T)$ made with an isotropic BCS expression.

field was estimated from the $M(H)$ curve at 0.5 K to be ≈10 Oe. From the field dependence of the resistivity data [13] the upper critical field $H_{c2}(0)$ was estimated to be 22.3(1) kOe, while the Pauli paramagnetic limit $18.4T_C = 66(2)$ kOe. Heat capacity, $C_P$, as a function of temperature for $0.45 \leqslant T \leqslant 5$ K is shown in figure 1(c) in different applied magnetic fields. In the normal state $C_P(T)$ was found to be independent of the external magnetic field. Above $T_C$ in the normal state, the $C_P(T)$ data can be described using $C_P(T) = \gamma T + \beta T^3$, where $\gamma$ is the electronic heat capacity coefficient, and $\beta T^3$ is the lattice (phonon) contribution to the specific heat. Fitting gives $\gamma = 5.56(1)$ mJ mol$^{-1}$ K$^{-2}$ and $\beta = 0.17(2)$ mJ mol$^{-1}$ K$^{-4}$. Using the Debye model, the Debye temperature is given by $\Theta_D = (\frac{12\pi^4}{5\beta} nR)^{1/3}$, where $R = 8.314$ J mol$^{-1}$ K$^{-1}$ is the gas constant and $n = 3$ is the number of atoms per formula unit in HfIrSi. Using this relationship, $\Theta_D$ is estimated to be 325(12) K. The jump in the heat capacity $\Delta C_P(T_C) = 28.5(1)$ mJ mol$^{-1}$ K$^{-1}$ and $T_C = 3.6(1)$ K, yields $\Delta C/\gamma T_C = 1.42(5)$ [13]. This value is close to 1.43 expected for weak-coupling BCS superconductors [24].

Figure 1(d) shows the temperature dependence of the electronic specific heat, $C_e(T)$, obtained by subtracting the phonon contribution from $C_P(T)$. $C_e(T)$ can be used to investigate the superconducting gap symmetry. From the fit to the exponential temperature dependence of $C_e(T)$ shown in figure 1(d), we find $\Delta(0) = 0.50(2)$ meV which is close to 0.51(1) meV obtained from the analysis of the TF-$\mu$SR data presented below. $\Delta(0) = 0.50(2)$ meV gives $2\Delta(0)/k_B T_C = 3.2(2)$, which is close to the value of 3.53 expected for weak-coupling BCS superconductors [25].

### 3.2. Transverse-field $\mu$SR measurements

To investigate the superconducting gap structure in *o*-HfIrSi, we have performed TF-$\mu$SR measurements. Figures 2(a) and (b) display the TF-$\mu$SR asymmetry spectra taken at temperatures above and below $T_C$ in an applied magnetic field of 300 Oe. The presence of a flux-line lattice (FLL) in the superconducting state results in an inhomogeneous field distribution within the sample, which in turn induces a faster decay in the asymmetry spectra below $T_C$ (figure 2(b)). The time evolution of the TF-$\mu$SR data at all temperatures above and below $T_C$ is best described by a sinusoidal oscillatory function damped with a Gaussian relaxation and an oscillatory background term [26–29]:

$$G_{z1}(t) = A_1 \cos(\omega_1 t + \varphi) \exp(-\frac{\sigma^2 t^2}{2}) + A_2 \cos(\omega_2 t + \varphi). \quad (1)$$

Here, $A_1 = 0.642(3)$ and $A_2 = 0.358(1)$ reflect the contributions to the initial asymmetry arising from the muons

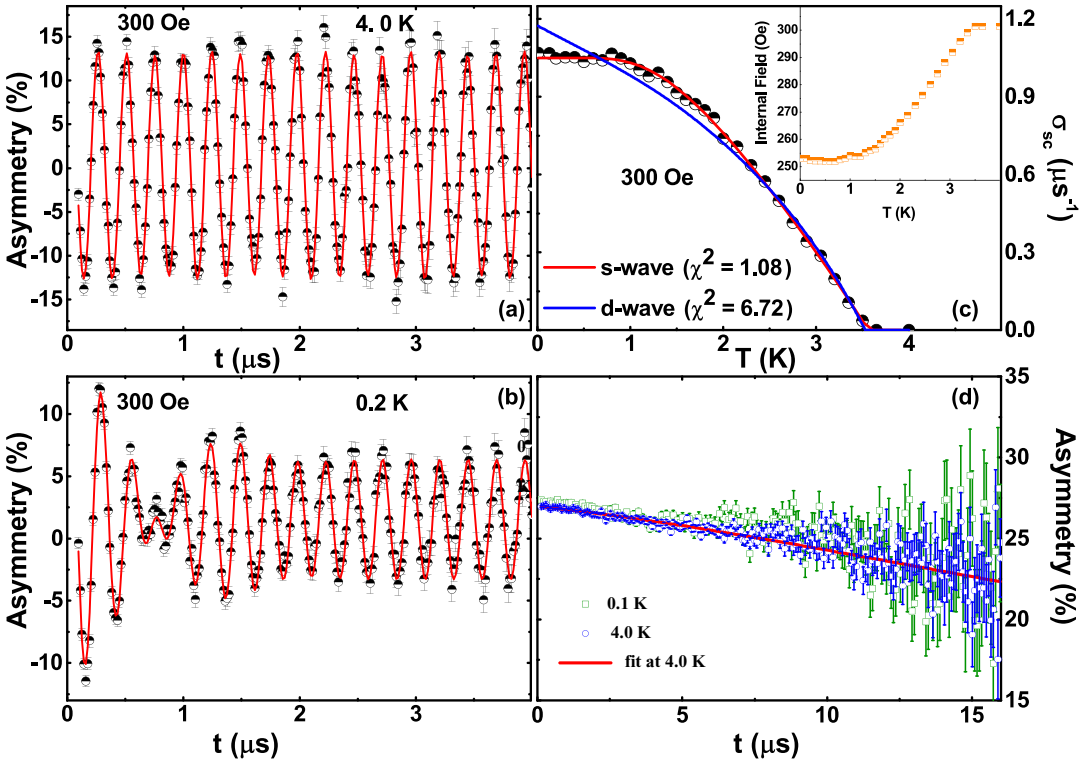


**Figure 2.** Time evolution of TF-$\mu$SR asymmetry spectra for HfIrSi recorded at (a) $T = 4.0$ K and (b) $T = 0.2$ K in a transverse magnetic field $H = 300$ Oe. The solid red line is a fit to the data using equation (1) as described in the text. (c) Temperature dependence of the superconducting depolarization rate $\sigma_{sc}(T)$ in the presence of an applied magnetic field of 300 Oe. The inset shows the temperature dependence of the internal field. (d) Zero-field $\mu$SR time spectra for HfIrSi collected at 0.1 K (green squares) and 4 K (blue circles) are shown together with a line that is a least squares fit to the data collected at 4 K using equation (3) (please see text for details).

implanted in the sample and from the muons implanted directly into the silver sample holder that do not depolarize, respectively. $\omega_1$ and $\omega_2$ are the muon precession frequencies within the sample and the sample holder, respectively, $\varphi$ is an initial phase of the offset, and $\sigma$ is the total muon spin relaxation rate. $\sigma$ consists of two contributions: one is due to the inhomogeneous field variation across the superconducting vortex lattice, $\sigma_{sc}$, and the other is a normal state contribution, $\sigma_n = 0.029\ \mu s^{-1}$, which is taken to be temperature independent over the entire temperature range studied and was obtained from spectra measured above $T_C$. Using $\sigma^2 = \sigma_{sc}^2 + \sigma_n^2$ we obtain the superconducting contribution $\sigma_{sc}$. The temperature variation of the penetration depth/superfluid density was modelled using [30–33]

$$\frac{\sigma_{sc}(T)}{\sigma_{sc}(0)} = \frac{\lambda^{-2}(T,\Delta_{0,i})}{\lambda^{-2}(0,\Delta_{0,i})}, \\ = 1 + \frac{1}{\pi}\int_0^{2\pi}\int_{\Delta(T)}^{\infty}\left(\frac{\delta f}{\delta E}\right)\times\frac{E\mathrm{d}E\mathrm{d}\phi}{\sqrt{E^2-\Delta(T,\Delta_i)^2}}, \quad (2)$$

where $f = [1+\exp(-E/k_BT)]^{-1}$ is the Fermi function and $\Delta_i(T,0) = \Delta_{0,i}\delta(T/T_C)g(\phi)$. $\Delta_{0,i}$ is the value of superconducting gap. The temperature dependence of the superconducting gap is approximated by the relation $\delta(T/T_C) = \tanh[1.82[1.018(T_C/T-1)]^{0.51}]$ where $g(\phi)$ refers to the angular dependence of the superconducting gap function. $g(\phi)$ is replaced by (a) 1 for an *s*-wave gap, and (b) $|\cos(2\phi)|$ for a *d*-wave gap with line nodes [34, 35]. The data is best modelled using a single isotropic *s*-wave gap of 0.51(1) meV, which yields a gap to $T_C$ ratio, $2\Delta/k_BT_C = 3.38(2)$ that is very close to the 3.3(2) obtained from the heat capacity data presented earlier, and indicates weak-coupling superconductivity in HfIrSi. The muon spin depolarization rate attributable to the superconducting state ($\sigma_{sc}$) is related with penetration depth via $\sigma_{sc}(T) = 0.0431\times\frac{\gamma_\mu\phi_0}{\lambda^2(T)}$, where $\phi_0 = 2.609\times10^{-15}$ Wb is the magnetic flux quantum. This gives $\lambda_L(0) = 259(4)$ nm for the *s*-wave fit. The London model provides a direct relation between $\lambda(T)$ and $(m^*/n_s)$ $\lambda_L^2 = m^*c^2/4\pi n_s e^2$ where $m^* = (1+\lambda_{e-ph})m_e$ is the effective mass in units of the electron rest mass $m_e$, and $n_s$ the carrier density. $\lambda_{e-ph}$ is calculated from $\Theta_D$ and $T_C$ use the McMillan equation $\lambda_{e-ph} = \frac{1.04+\mu^*\ln(\Theta_D/1.45T_C)}{(1-0.62\mu^*)\ln(\Theta_D/1.45T_C)-1.04}$. The superconducting carrier density is then estimated to be $n_s = 6.6(1)\times10^{26}$ carriers m$^{-3}$ and the effective-mass enhancement $m^* = 1.57(3)m_e$, for HfIrSi. Details of similar calculations can be found in [36–41]

### 3.3. Zero-field $\mu$SR measurements

ZF-$\mu$SR measurements were performed to check for the appearance of spontaneous magnetic fields in the superconducting state of HfIrSi. The time evolution of the zero-field asymmetry spectra above (4 K) and below (0.1 K) $T_C$ are

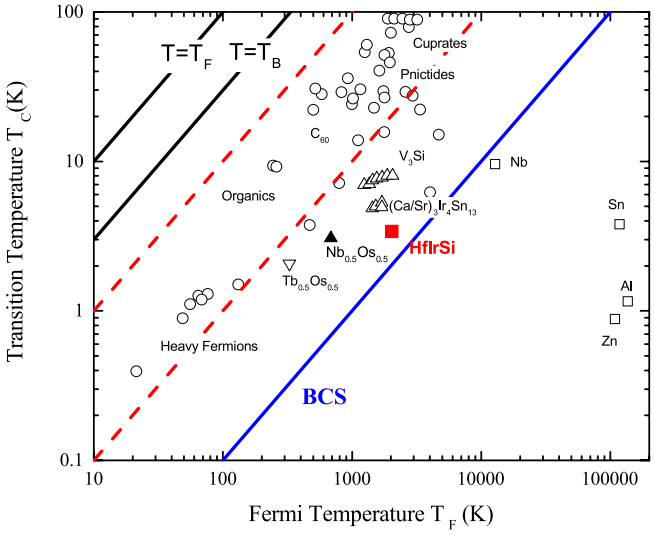


**Figure 3.** The superconducting transition temperature, $T_C$, versus the effective Fermi temperature, $T_F$, where the position of HfIrSi is shown by the solid red square. The unconventional superconductors fall within a band indicated by the red dashed lines for which $1/10 \geqslant (T_C/T_F) \geqslant 1/100$.

shown in figure 2(d). The ZF-$\mu$SR data are well described using a damped Gaussian Kubo–Toyabe (KT) function, and a background term arising from muons that miss the sample and stop in the silver sample plate,

$$G_{z2}(t) = A_3 G_{KT}(t) e^{-\lambda_\mu t} + A_{bg}. \quad (3)$$

Here $G_{KT}(t)$ is the Gaussian Kubo–Toyabe function given by $G_{KT}(t) = [\frac{1}{3} + \frac{2}{3}(1 - \sigma_{KT}^2 t^2) \exp(-\frac{\sigma_{KT}^2 t^2}{2})]$. $A_3$ and $A_{bg}$ are the asymmetries arising from the sample and background, respectively. $\sigma_{KT}$ and $\lambda_\mu$ are the muon spin relaxation rates due to randomly oriented nuclear moments. The fitting parameters $A_3$, $A_{bg}$ are independent of temperature. Fits to the ZF-$\mu$ SR asymmetry data using equation (3) are shown by the solid lines in figure 2(d) and give $\sigma_{KT} = 0.068(1)$ $\mu s^{-1}$ and $\lambda_\mu = 0.0046(2)$ $\mu s^{-1}$ at 0.1 K and $\sigma_{KT} = 0.064(1)$ $\mu s^{-1}$ and $\lambda_\mu = 0.0046(1)$ $\mu s^{-1}$ at 4 K. The values of $\sigma_{KT}$ and $\lambda_\mu$ above and below $T_C$ are very similar, and there is no clear change in either parameter at the superconducting transition temperature, indicating that TRS is preserved in the superconducting state of HfIrSi.

### 3.4. Uemura classification scheme

The Uemura classification scheme [42, 43] correlates the $T_C$ and the effective Fermi temperature, $T_F$ ( $= \frac{\hbar^2 (3\pi^2)^{2/3} n_s^{2/3}}{2 k_B m^*}$) of a superconductor. The values of $n_s$ and $m^*$ have been estimated from the TF-$\mu$SR data. In this classification unconventional superconductors lie between $1/10 \geqslant (T_C/T_F) \geqslant 1/100$, while for conventional BCS superconductors $T_C/T_F \leqslant 1/1000$. The position of HfIrSi indicates it is a conventional superconductor with its $T_C/T_F$ value of 3.6(1)/2320(10) = 0.00155(5).

### 3.5. Theoretical investigations

The Vienna *ab initio* Simulation Package (VASP) [44] was used to perform density-functional theory (DFT) electronic structure calculations on HfIrSi. The projected augmented wave (PAW) pseudo-potentials were used to describe the core electrons, with the Perdew–Burke–Ernzerhof (PBE) functional [45] used for the exchange-correlation potential. The cut-off energy for the plane-wave basis set was fixed at 500 eV. The Monkhorst–Pack $k$-mesh was set to $14 \times 14 \times 14$ in the Brillouin zone for the self-consistent calculations.

HfIrSi is orthorhombic (*Pnma*(62) space group) with *mmm* point group symmetry. The relaxed lattice parameters obtained are $a = 6.499$ Å, $b = 3.944$ Å, $c = 7.376$ Å and $\alpha = \beta = \gamma = 90°$. Typically, it is observed that band structure calculated with relaxed coordinates, rather then experimentally determined lattice parameters, give better agreement with experiments. Here, the difference between the the relaxed coordinates and the experimentally determined lattice parameters is very small and experimental ones is very small and the corresponding band structures are not significantly different. To deal with the strong correlation effects of the $d$-electrons of the Ir atoms, the LDA+U method [46, 47] was employed with $U = 2.8$ eV. For the Fermi surface and density of states calculations, a larger $k$-mesh of $31 \times 31 \times 31$ was used. The calculations were repeated with SOC but this produced no significant change in the low-energy spectrum.

Due to the involvement of the strongly correlated transition metals as well as possible SOC, one may anticipate that the superconductivity in HfIrSi may be exotic. However, the observation of conventional, time-reversal invariant superconductivity leads to the question: how does a phonon mediated attractive potential win out over the strong Coulomb interaction to give conventional superconductivity? Our investigation favours a conventional pairing symmetry based on the observations of fully gapped superconductivity and weak correlation strength in this material.

To address this point, we investigate the DFT band structure as shown in figure 4. From the partial-DOS shown in figure 4(a), we find that the transition metals Ir and Hf have nearly equal weight in the low-energy spectrum, and contribute most to the total DOS. Additionally, both transition metals have the corresponding 4$d$ and 5$d$ orbitals, respectively providing the dominant contribution to the Fermi surfaces. The result indicates that these two atoms both undergo strong hybridization in this system. This is confirmed by the visualization of the orbital weight distributions of the electronic structure as shown in figure 4(b). We plot here the difference in the orbital weights between the Ir-$d$ and Hf-$d$ orbitals. We find that the bands near the Γ-point are dominated by the Hf-$d$ orbitals while the Ir-$d$ atoms contribute strongly to those near Z (on the $k_z = \pm\pi$-plane). This result indicates that the Hf and Ir atoms hybridize rather strongly along the $c$-axis of the lattice. This hybridization is responsible for the strong three-dimensionality of this system which screens the Coulomb

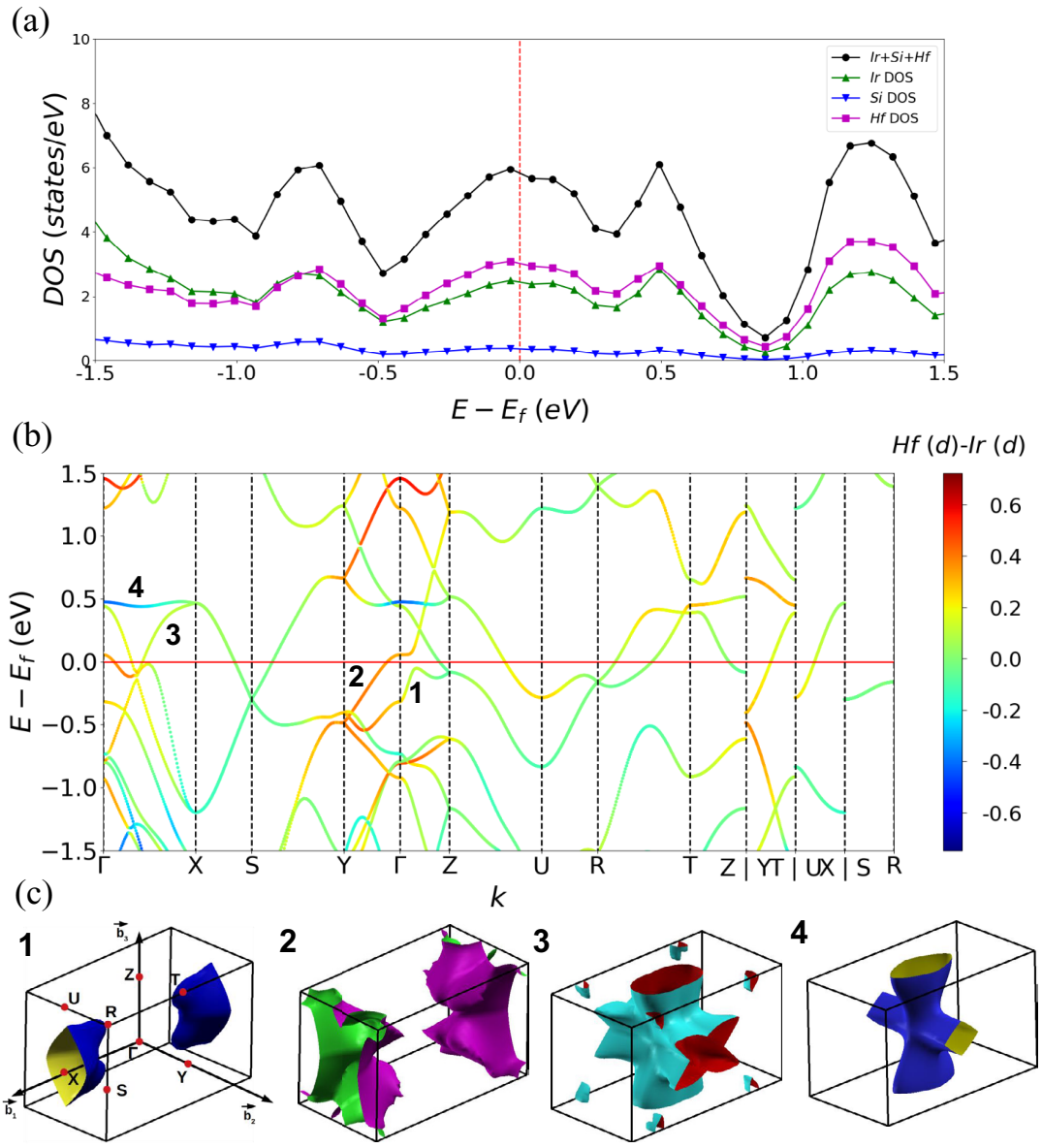


**Figure 4.** (a) Computed partial DOS for Hf, Ir, and Si atoms, along with the total DOS. We clearly observe that the Hf and Ir atoms contribute dominantly to the low-energy spectrum. For both these atoms, outermost *d*-orbitals contribute mostly to this energy scale. (b) DFT calculation of the band structure along with the standard high-symmetry directions for the orthorhombic crystal structure of HfIrSi. The band structure is coloured with a gradient colour map where blue indicates Ir-*d* orbitals and red shows the Hf-*d* orbitals. (c) Corresponding four Fermi surfaces in the 3D Brillouin zone. The colours on the Fermi surfaces have no significance here. Four Fermi surfaces are denoted by '1', '2', '3', and '4'. The result indicates that the bands near the Γ-point are dominated by Hf-*d* states while those near the 'Z' point gain more weight from the Ir-*d* states.

interaction. As a result, despite the presence of *d* electrons in this systems, the correlation effect is weakened, leading to the electron-phonon coupling increasing in importance [48].

The Fermi surface topologies shown in figure 4(c) confirm the strong three-dimensionality in all four bands. We consistently find two Fermi pockets near the Γ-points and two Fermi pockets centering on the X-points. The large Fermi surface volume is consistent with the high carrier density of this system as measured in the $\mu$SR experiments, and the higher value of the Fermi temperature presented in figure 3. These results are also consistent with the weak correlation strength in this system [49]. Strong three-dimensionality can also reduce relativistic effects, weakening the SOC.

## 4. Comments and perspectives

We have performed magnetization, heat capacity, and ZF and TF-$\mu$SR measurements at temperatures above and below $T_C$ on the orthorhombic 111 superconductor HfIrSi. The heat-capacity and magnetization data confirm bulk superconductivity in this material with a $T_C = 3.6(1)$ K. The temperature dependence of muon depolarization rate, $\sigma_{sc}(T)$, determined from the TF-$\mu$SR data collected in the field-cooled mode, is best fit by an isotropic *s*-wave model. The value of $2\Delta(0)/k_BT_C = 3.38(2)$ obtained from the *s*-wave gap fit, suggests weak-coupling BCS-type superconductivity in HfIrSi. The ZF-$\mu$SR measurements reveal no sign of any spontaneous

field appearing below $T_C$ which suggests that TRS is preserved in HfIrSi. Electronic structure calculations suggest that the Hf and Ir atoms in HfIrSi hybridize strongly along the *c*-axis, and that this hybridization is responsible for the strong three-dimensionality of the system which screens the Coulomb interaction. As a result, despite the presence of *d*-electrons in this systems, the correlation effects are weakened, meaning that the electron-phonon coupling gains in importance. To date, a large number of equiatomic $MM'X$ compounds have been discovered with high superconducting transition temperatures and high critical magnetic fields, but $\mu$SR investigations have been carried out on just a few of these 111 compounds. The present study provides a valuable comparison for future $\mu$SR investigations on this family of compounds. The present results will also help in the development of realistic theoretical models, including the role of strong spin–orbit coupling, that explain the origin of superconductivity in HfIrSi, and also may help us arrive at empirical criteria for the occurrence of superconductivity with strong SOC, high $T_c$, and $H_{c2}$ in other $MM'X$ equiatomic ternary systems.

## Acknowledgments

AB would like to acknowledge the Department of Science and Technology (DST) India, for an Inspire Faculty Research Grant (DST/INSPIRE/04/2015/000169), and the UK-India Newton grant for funding support. KP acknowledge the financial support from DST India, for Inspire Fellowship (IF170620). DTA would like to thank the Royal Society of London for the UK-China Newton funding and the Japan Society for the Promotion of Science for an invitation fellowship. TD acknowledges the financial support from the Science and Engineering Research Board (SERB), Department of Science & Technology (DST), Govt. of India for the Start-Up Research Grant (Young Scientist).

## ORCID iDs

A Bhattacharyya https://orcid.org/0000-0002-8037-0487
K Panda https://orcid.org/0000-0003-4305-9566
D T Adroja https://orcid.org/0000-0003-2280-079X
P K Biswas https://orcid.org/0000-0002-7367-5960
Tanmoy Das https://orcid.org/0000-0003-1881-9164
M R Lees https://orcid.org/0000-0002-2270-2295
A D Hillier https://orcid.org/0000-0002-2391-8581

## References

[1] Barz H, Ku H C, Meisner G P, Fisk Z and Matthias B T 1980 *Proc. Natl Acad. Sci.* **77** 3132
[2] Müller R, Shelton R N, Richardson J W and Jacobson R A 1983 *J. Less-Common Met.* **42** 177
[3] Meisner G P, Ku H C and Barz H 1983 *Matter. Res. Bull.* **18** 983
[4] Keiber H, Wühl H, Meisner G P and Stewart G R 1984 *J. Low Temp. Phys.* **55** 11
[5] Shirotani I, Ichihashi N, Nozawa K, Kinoshita M, Yagi T, Suzuki K and Enoki T 1993 *Japan. J. Appl. Phys.* **32–3** 695
[6] Shirotani I, Tachi K, Takeda K, Todo S, Yagi T and Kanoda K 1995 *Phys. Rev.* B **52** 6197
[7] Seo D K, Ren J, Whangbo M H and Canadell E 1997 *Inorg. Chem.* **36** 6058–63
[8] Shirotani I, Konno Y, Okada Y, Sekine C, Tado S and Yagi T 1998 *Solid State Commun.* **108** 967
[9] Shirotani I, Tachi K, Konnon Y, Todo S and Yagi T 1999 *Phil. Mag.* B **79** 767–76
[10] Shirotani I, Takeya M, Kaneko I, Sekine C and Yagi T 2000 *Solid State Commun.* **116** 683
[11] Shirotani I, Takaya M, Kaneko I, Sekine C and Yagi T 2001 *Physica* C **357–60** 329
[12] Ching W Y, Xu Y N, Ouyang L and Wong-Ng W 2003 *J. Appl. Phys.* **93** 8209
[13] Kase N, Suzuki H, Nakano T and Takeda N 2016 *Supercond. Sci. Technol.* **29** 035011
[14] Kita T and Arai M 2004 *Phys. Rev.* B **70** 224522
[15] Wong-Ng W, Ching W Y, Xu Y N, Kaduk J A, Shirotani I and Swartzendruber L 2003 *Phys. Rev.* B **67** 144523
[16] Wang X-Z, Chevalier B, Etourneau J and Hagenmuller P 1985 *Mater. Res. Bull.* **20** 517
[17] Bhattacharyya A, Adroja D T, Quintanilla J, Hillier A D, Kase N, Strydom A M and Akimitsu J 2015 *Phys. Rev.* B **91** 060503
[18] Bhattacharyya A, Adroja D T, Kase N, Hillier A D, Akimitsu J and Strydom A M 2015 *Sci. Rep.* **5** 12926
[19] Bhattacharyya A, Adroja D T, Kase N, Hillier A D, Strydom A M and Akimitsu J 2018 *Phys. Rev.* B **98** 024511
[20] Yuan H Q, Agterberg D F, Hayashi N, Badica P, Vandervelde D, Togano K, Sigrist M and Salamon M B 2006 *Phys. Rev. Lett.* **97** 017006
[21] Sonier J E, Brewer J H and Kiefl R F 2000 *Rev. Mod. Phys.* **72** 769
[22] Lee S L, Kilcoyne S H and Cywinski R 1999 *Muon Science: Muons in Physics, Chemistry and Materials* (Bristol, UK: SUSSP and IOP)
[23] Pratt F L 2000 *Physica* B **289–90** 710
[24] Tinkham M 1975 *Introduction to Superconductivity* (New York: McGraw-Hill)
[25] Bardeen J, Cooper L N and Schrieffer J R 1957 *Phys. Rev.* **106** 162
[26] Bhattacharyya A, Adroja D T, Smidman M and Anand V K 2018 *Sci. China-Phys. Mech. Astron.* **61** 127402
[27] Adroja D T, Bhattacharyya A, Biswas P K, Smidmann M, Hillier A D, Mao H, Luo H, Cao G H, Wang Z and Wang C 2017 *Phys. Rev.* B **96** 144502
[28] Bhattacharyya A, Adroja D T, Panda K, Saha S, Das T, Machado A J S, Grant T W, Fisk Z, Hillier A D and Manfrinetti P 2019 *Phys. Rev. Lett.* **122** 147001
[29] Anand V K, Britz D, Bhattacharyya A, Adroja D T, Hillier A D, Strydom A M, Kockelmann W, Rainford B D and McEwen K A 2014 *Phys. Rev.* B **90** 014513
[30] Prozorov R and Giannetta R W 2006 *Supercond. Sci. Technol.* **19** R41
[31] Adroja D T, Bhattacharyya A, Telling M, Feng Y, Smidman M, Pan B, Zhao J, Hillier A D, Pratt F L and Strydom A M 2015 *Phys. Rev.* B **92** 134505
[32] Adroja D T, Bhattacharyya A, Smidman M, Hillier A D, Feng Y, Pan B, Zhao J, Lees M R, Strydom A M and Biswas P K 2017 *J. Phys. Soc. Japan* **86** 03470
[33] Bhattacharyya A, Adroja D T, Hillier A D, Jha R, Awana V P S and Strydom A M 2017 *J. Phys: Condens. Matter.* **29** 265602
[34] Pang G, Smidman M, Jiang W, Bao J, Weng Z, Wang Y, Jiao L, Zhang J, Cao G and Yuan H 2015 *Phys. Rev.* B **91** 220502
[35] Annett J F 1989 *Adv. Phys.* **39** 83–126
[36] Brandt E H 2003 *Phys. Rev.* B **68** 054506

[37] Chia E E, Salamon M, Sugawara H and Sato H 2004 *Phys. Rev.* B **69** 180509
[38] Amato A 1997 *Rev. Mod. Phys.* **69** 1119
[39] McMillan W L 1968 *Phys. Rev.* **167** 331
[40] Bhattacharyya A, Adroja D T, Biswas P K, Sato Y J, Lees M R, Aoki D and Hillier A D 2020 *J. Phys.: Condens. Matter* **32** 065602
[41] Das D, Gupta R, Bhattacharyya A, Biswas P K, Adroja D T and Hossain Z 2018 *Phys. Rev.* B **97** 184509
[42] Uemura Y J *et al* 1989 *Phys. Rev. Lett.* **62** 2317
[43] Hillier A D and Cywinski R 1997 *Appl. Mag. Reson.* **13** 95
[44] Kresse G and Hafner J 1993 *Phys. Rev.* B **47** 558
Kresse G and Hafner J 1994 *Phys. Rev.* B **49** 14251
Kresse G and Furthmüller J 1996 *Comput. Mat. Sci.* **6** 15
Kresse G and Furthmüller J 1996 *Phys. Rev.* B **54** 11169
[45] Perdew J P, Burke K and Matthias E 1996 *Phys. Rev. Lett.* **77** 18
[46] Liechtenstein A I, Anisimov V I and Zaanen J 1995 *Phys. Rev.* B **52** 8
[47] Dudarev S L, Botton G A, Savrasov S Y, Humphreys C J and Sutton A P 1998 *Phys. Rev.* B **57** 3
[48] Das T and Dolui K 2015 *Phys. Rev.* B **91** 094510
Yin Z P, Kutepov A and Kotliar G 2013 *Phys. Rev.* X **3** 021011
[49] Das T, Markiewicz R S and Bansil A 2014 *Adv. Phys.* **63** 151–266